Supplementary Materials for

Annealing synchronizes the 70*S* ribosome into a minimum-energy conformation

Authors: Xiaofeng Chu[1,2†], Xin Su[1,3†], Mingdong Liu[1,4,5†], Li Li[3], Tianhao Li[1,4], Yicheng Qin[1], Guoliang Lu[3], Lei Qi[2], Yunhui Liu[1], Jinzhong Lin[3], Qing-Tao Shen[1,2*]

Affiliations:

[1]iHuman Institute and School of Life Science and Technology, ShanghaiTech University, Shanghai 201210, China.

[2]Laboratory for Marine Biology and Biotechnology, Qingdao National Laboratory for Marine Science and Technology, Qingdao 266237, China.

[3]State Key Laboratory of Genetic Engineering, School of Life Sciences, Zhongshan Hospital, Fudan University, Shanghai, 200438, China.

[4]University of Chinese Academy of Sciences, Beijing 100049, China.

[5]Shanghai Institute of Biochemistry and Cell Biology, Center for Excellence in Molecular Cell Science, Chinese Academy of Science, Shanghai, 200031, China.

[†]These authors contributed equally: Xiaofeng Chu, Xin Su, Mingdong Liu

[*]Corresponding author: Qing-Tao Shen

Email: Qing-Tao Shen (shenqt@shanghaitech.edu.cn)

This PDF file includes:

Supplementary Text:

Structural comparison of 70*S* ribosomes under various conditions

In our work, 70*S* ribosomes under various conditions were resolved via single-particle cryo-EM. Corresponding structural comparisons indicated that annealing could synchronize 70*S* ribosomes, especially flexible regions, into homogenous states with improved local resolution. To objectively compare 70*S* ribosomes, we tested reconstruction as follows:

1) Same batch of ribosomes. 70*S* ribosomes were aliquoted and stored at −80°C and unused ribosomes were discarded after thawing.

2) Same data collection conditions. The same microscope (Titan Krios G^{3i}) with the same camera (Gatan K3 BioQuantum) was used for all data collections. Total electron dose, defocus, and other pertinent values were set to be the same.

3) Same data processing pipeline. The procedure as described in the *SI Appendix*, Fig. S2*A* was consistently applied to all 70*S* ribosomes under various conditions.

4) Same data screening strategy. Only obvious junk and disassembled ribosomes were removed from the dataset. In most datasets, 82.3% to 93.7% of the particles were selected after 2D and 3D classifications. Three exceptions were the heated ribosome (S2) and annealed ribosomes (S9 and S10). Ribosomes (S9 and S10) were heated to 55°C and 65°C, respectively (closer to the ~72°C melting temperature of bacterial ribosome), for 5 min; these 70*S* ribosomes readily fell apart. Regarding the protocol S2, ribosomes were vitrified at 37°C as the heated state. Compared with ribosomes under other conditions, more unsatisfactory particles (~46.9%) were excluded from the final reconstruction, but the local resolution of 30*S* subunit was still inferior.

5) Same number of particles (200,000) for the final reconstruction, for comparison.

6) Repeating experiments. Repeats were performed on three representative conditions, including the unannealed (S1), heated (S2), and annealed (S5) ribosomes. A new batch of 70*S* ribosomes was used and reconstructed. There was no obvious structural difference between two parallel experiments.

In summary, the structural differences should be attributable to differences in treatments.

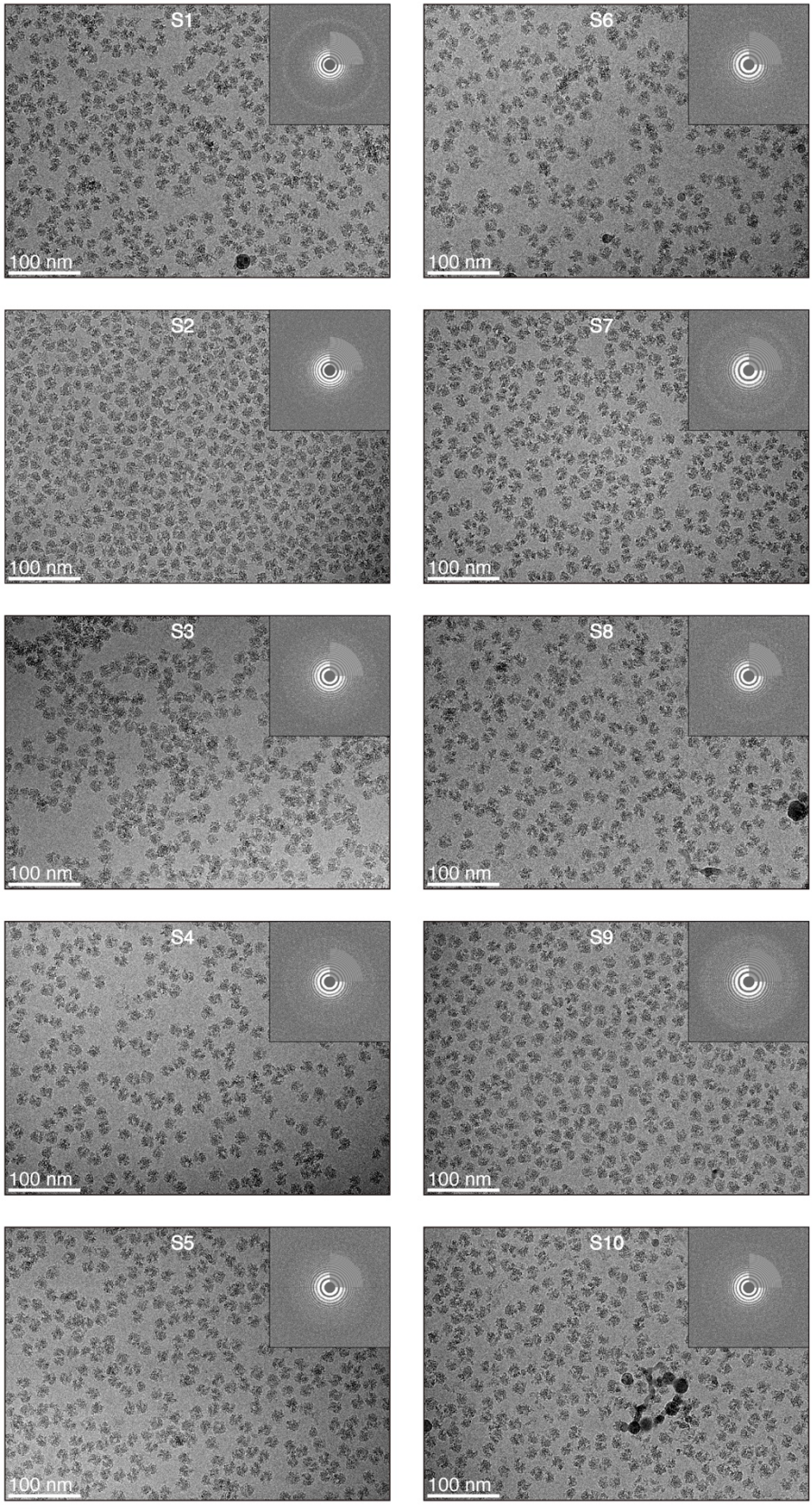
S1
100 nm
S6
100 nm
S2
100 nm
S7
100 nm
S3
100 nm
S8
100 nm
S4
100 nm
S9
100 nm
S5
100 nm
S10
100 nm

Figure S1. Typical cryo-EM images under various conditions and their respective power spectra Fig. 2*B* lists detailed conditions for protocols S1–S10.

A

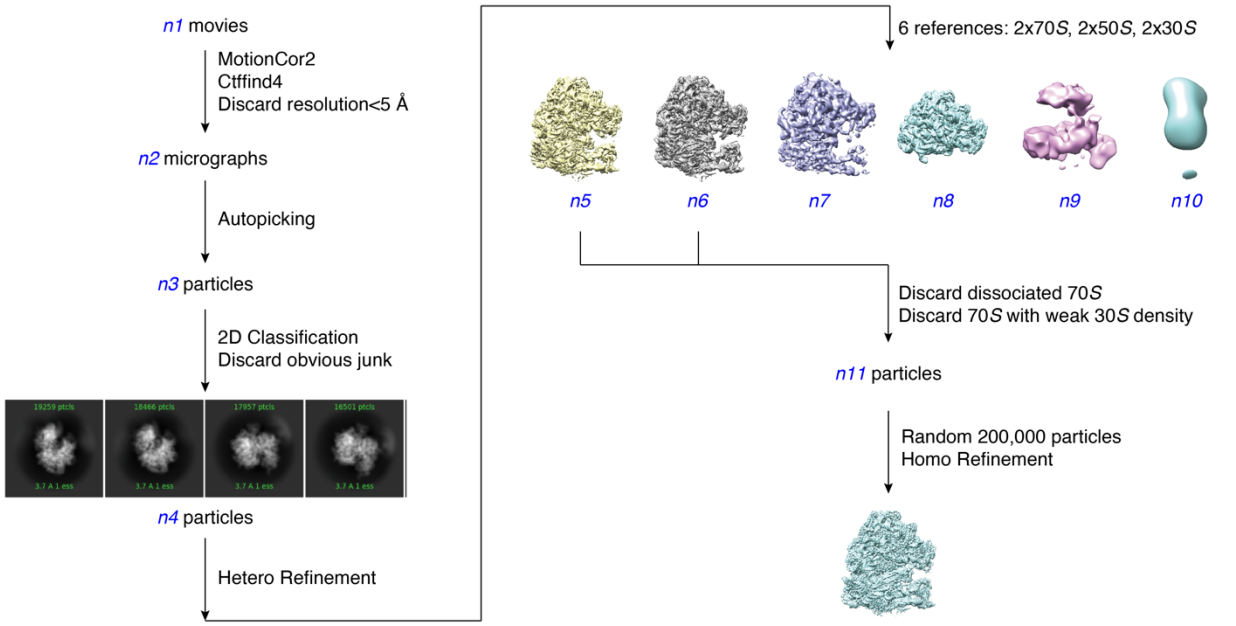

B

	Movies	Micro-graphs	Picked particles	2D classification	References for 3D classification							Ratio *n11*/*n4*	EMDB ID
					70*S*	70*S*	50*S*	50*S*	30*S*	30*S*	Selected		
	n1	*n2*	*n3*	*n4*	*n5*	*n6*	*n7*	*n8*	*n9*	*n10*	*n11*		
S1	5,438	5,197	1,129,669	897,050	442,399	309,892	8,928	132,634	294	2,903	752,291	83.9%	31266
S2	5,056	4,239	1,486,810	1,043,834	554,307	392,667	15,736	60,247	11,985	8,892	554,307	53.1%	31267
S3	7,593	6,257	1,076,160	667,543	252,162	299,175	83,972	16,601	7,458	8,175	551,337	82.6%	31268
S4	2,427	1,920	426,817	317,444	185,639	98,005	4,189	27,012	747	1,852	283,644	89.4%	31269
S5	3,606	2,856	647,109	580,225	287,649	189,665	4,469	98,254	126	62	477,314	82.3%	31270
S6	3,421	2,667	798,704	374,075	242,515	103,222	1,417	25,786	618	517	345,737	92.4%	31271
S7	2,717	1,541	315,619	242,490	89,942	137,174	2,255	12,242	481	396	227,116	93.7%	31272
S8	3,539	2,955	696,964	530,198	154,287	312,551	4,521	44,268	2,752	11,819	466,838	88.0%	31273
S9	3,732	3,102	998,953	763,444	508,021	82,446	158,699	12,861	1,169	248	508,021	66.5%	31274
S10	2,362	1,959	526,097	413,784	126,536	103,482	12,995	167,183	1,417	2,171	230,018	55.6%	31275

Figure S2. 3D reconstructions of 70*S* ribosomes under various conditions

(*A*) The same flow chart was used for 3D reconstruction of 70*S* ribosomes under various conditions. (*B*) Detailed numbers from *n1*–*n11* in (*A*) and the corresponding deposited EMDB IDs are listed.

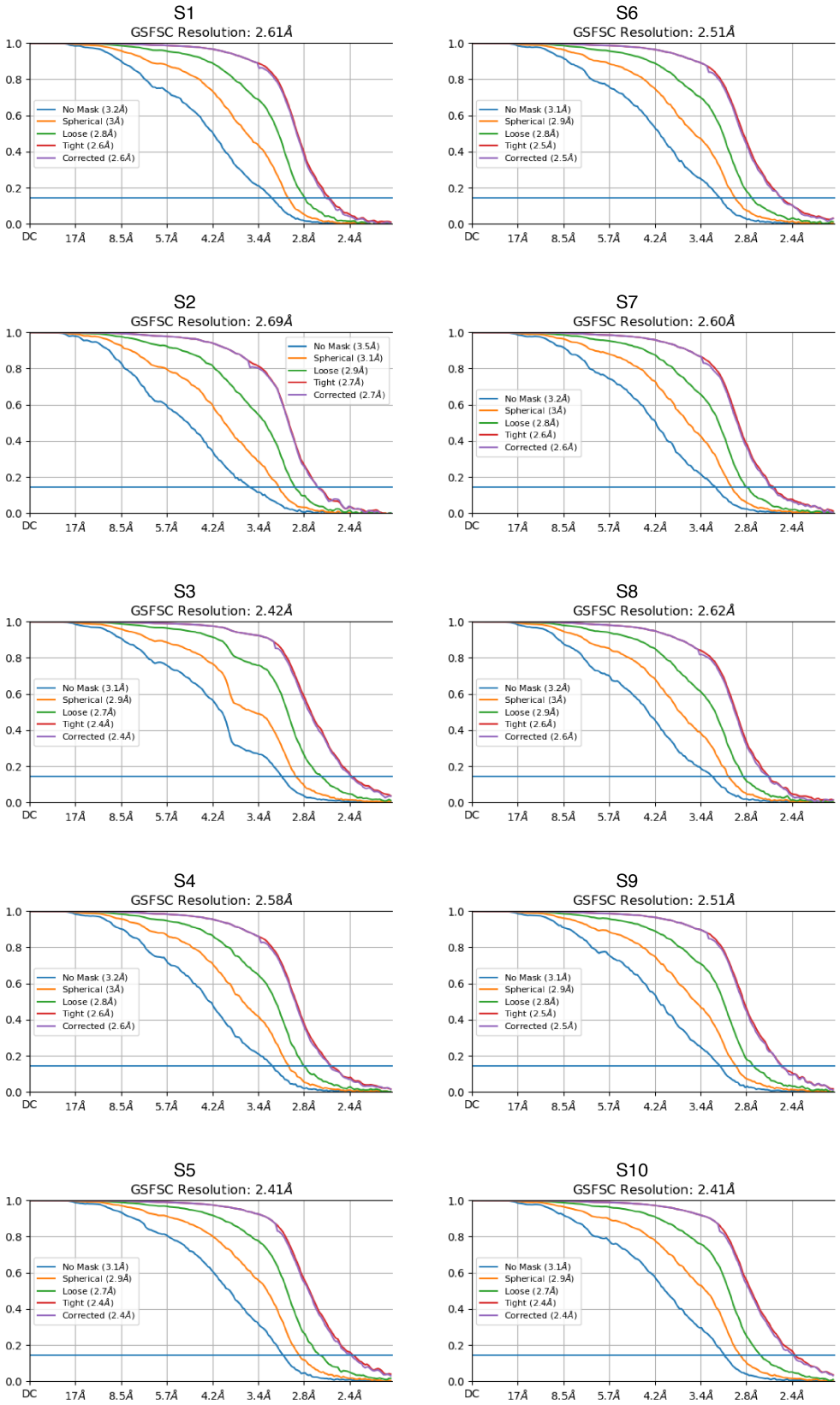

Figure S3. FSC curves for 70*S* ribosomes under various conditions

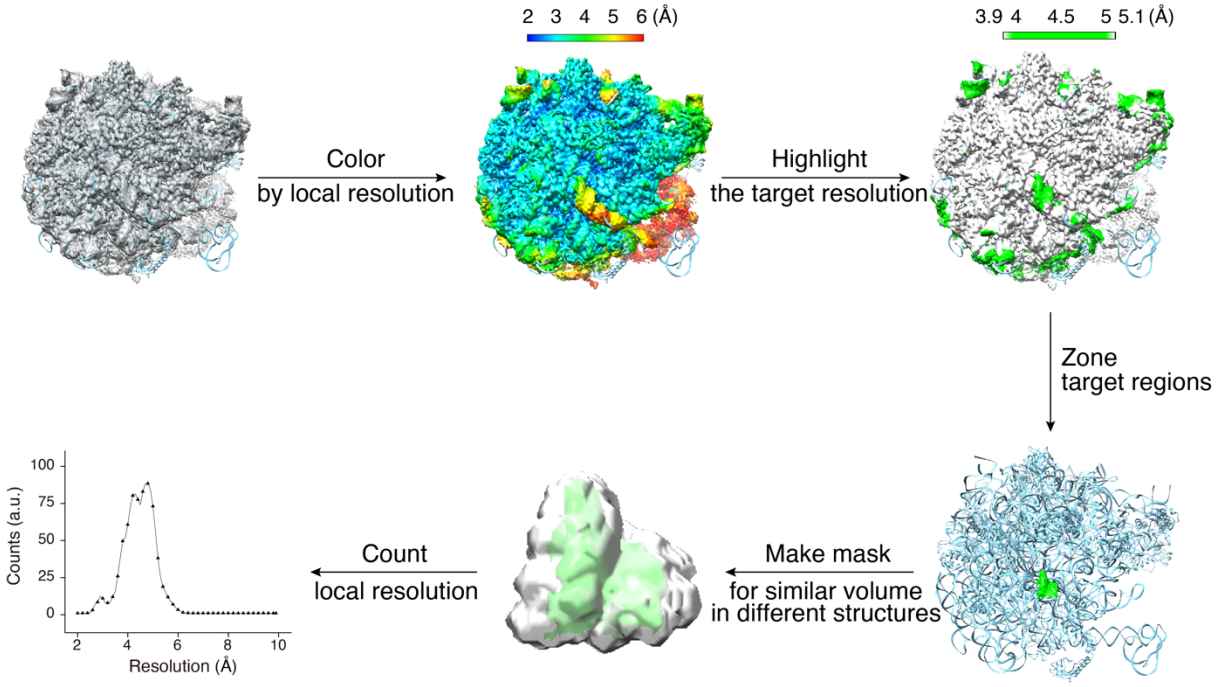

Figure S4. Flow chart for local resolution calculation on selected regions

To compare local resolutions from different structures, the volumes of the target regions in different EM maps were adjusted to the same level via changing thresholds.

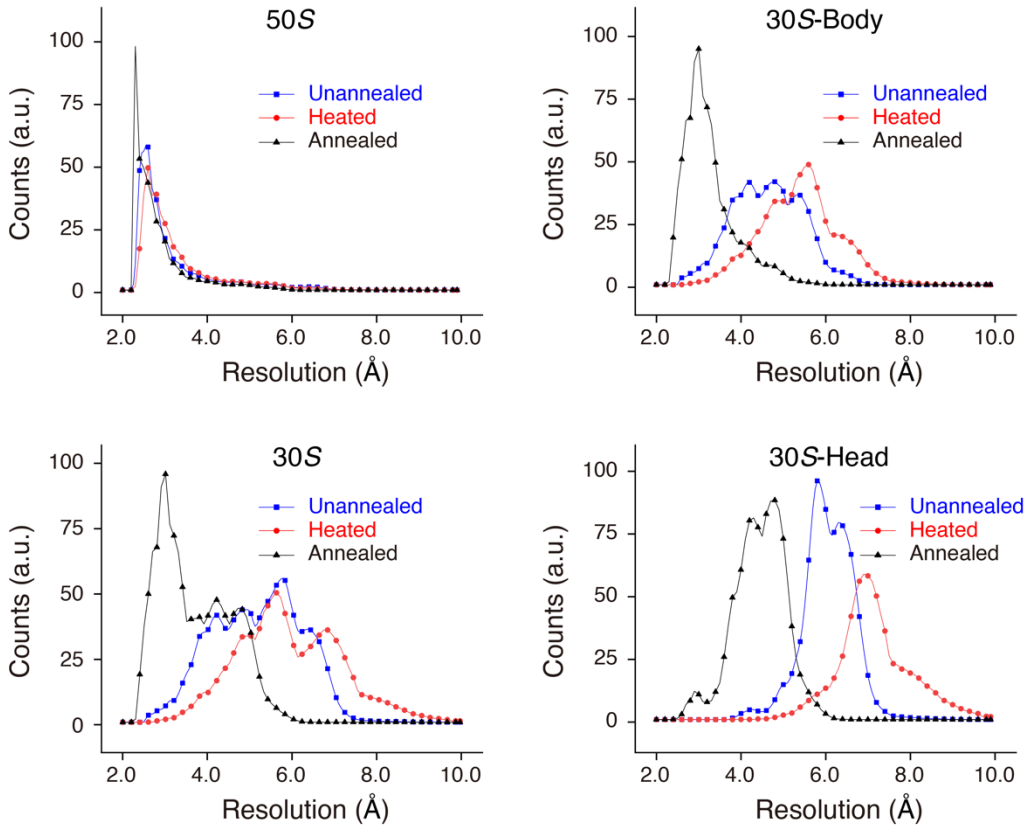

Figure S5. Local resolution histograms of different subdomains from the unannealed, heated, and annealed 70*S* ribosomes

The mean and standard deviation from these histograms were calculated (Fig. 1*B*). "a.u." means arbitrary units.

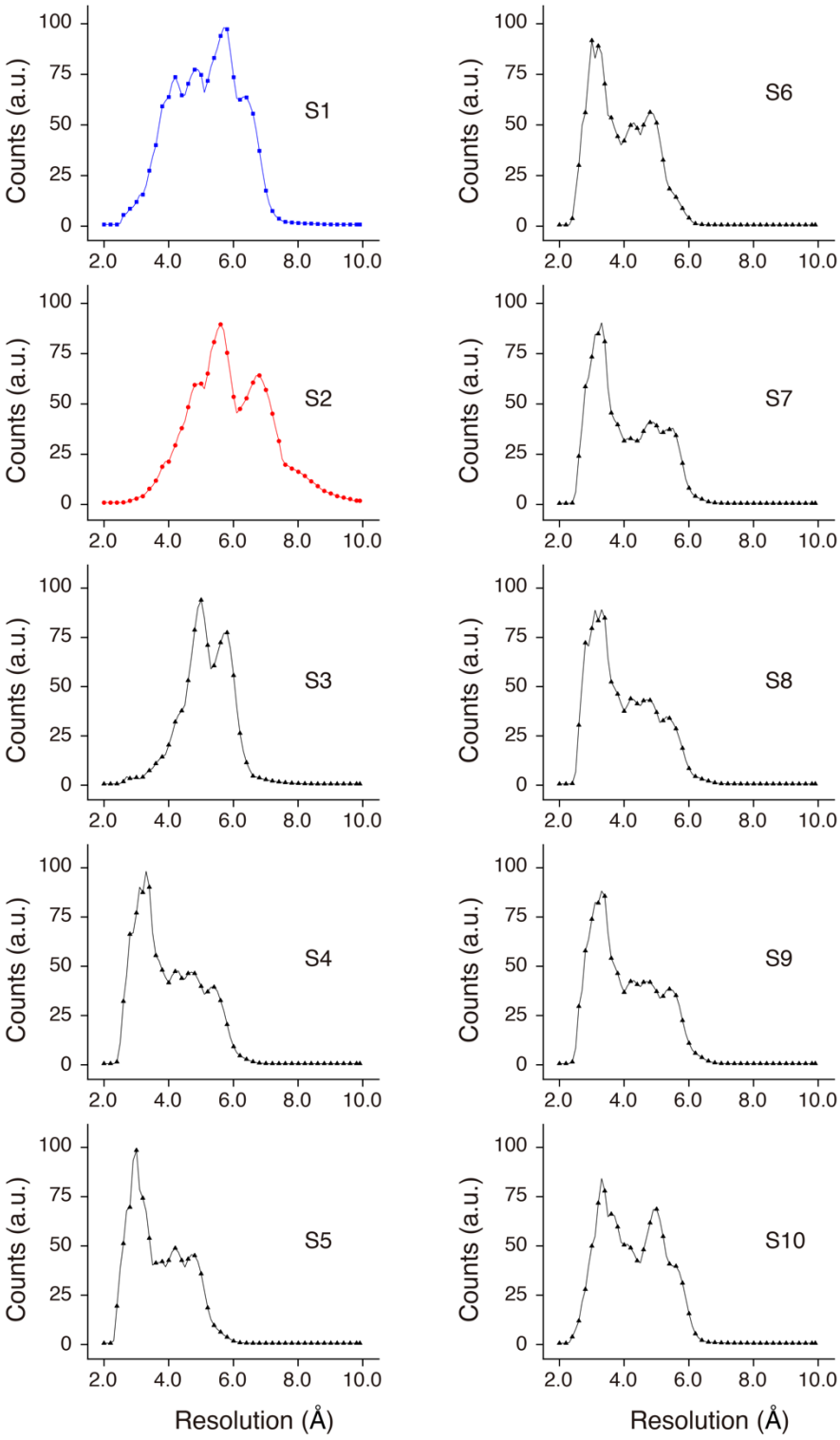

Figure S6. Local resolution histograms of 30*S* subunits under various conditions The mean and standard deviation from these histograms were calculated (Fig. 2*C*).

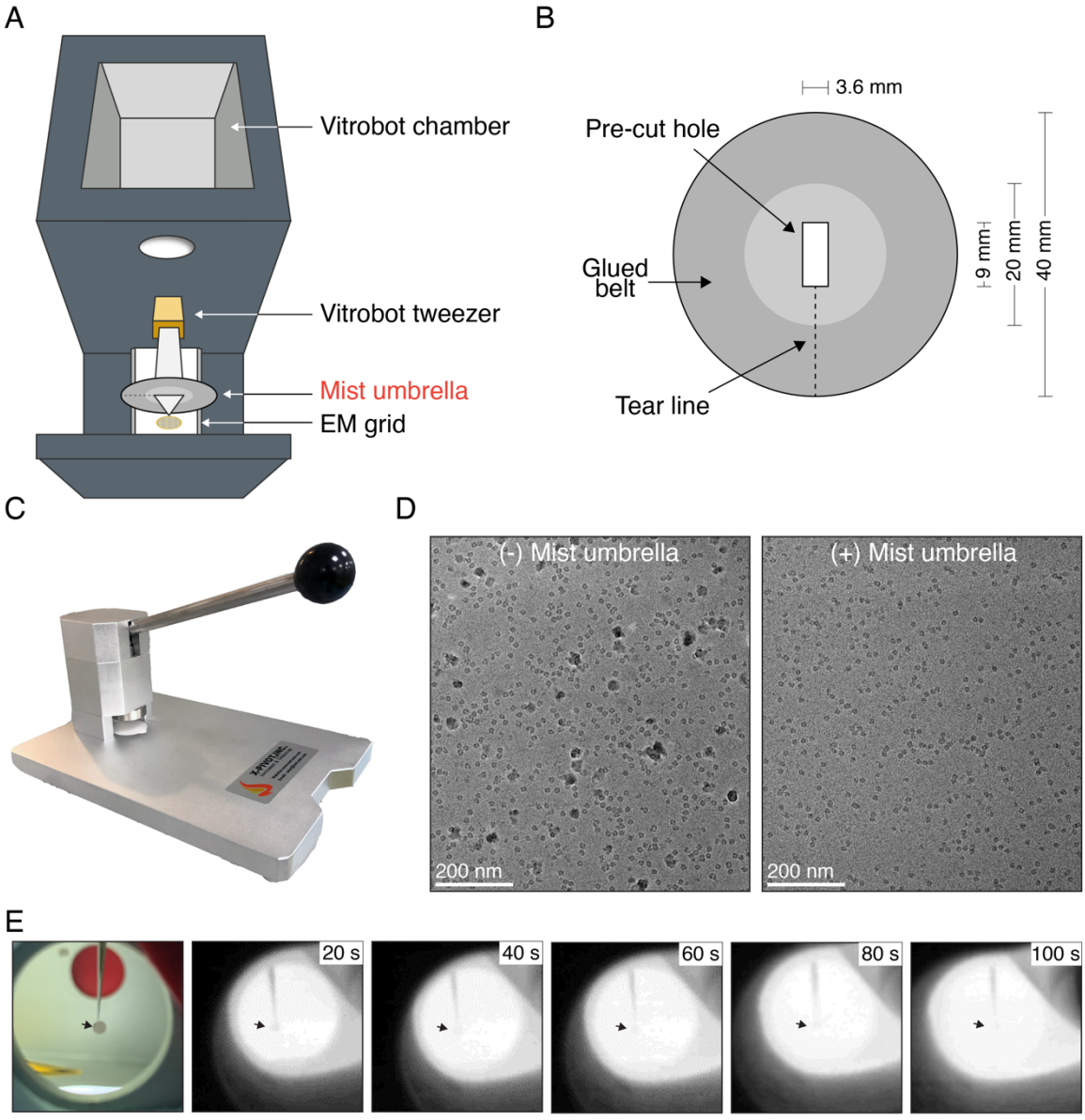

Figure S7. Optimization for temperature-dependent cryo-EM

(*A*) Diagram for the Vitrobot device with a mist umbrella. (*B*) Detailed parameters for the mist umbrella. Briefly, there is a pre-cut hole on round filter paper. (*C*) Home-made device to fabricate mist umbrellas. (*D*) Cryo-EM micrographs with or without a mist umbrella. (*E*) Heat exchange between grids and the Vitrobot chamber reached a balance in ~100 s. Black arrow points to the position of the cryo-EM grid.

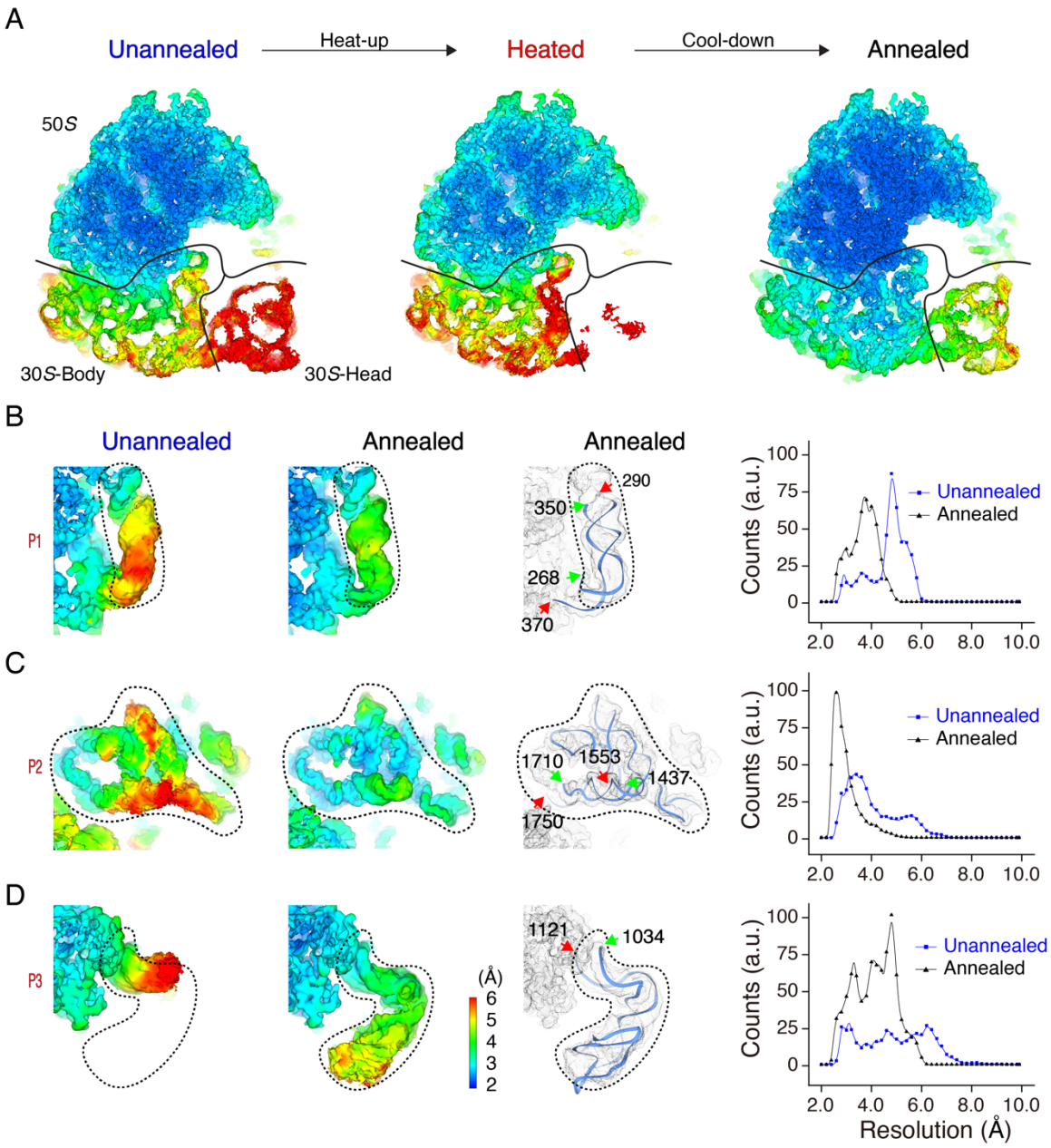

Figure S8. Annealing stabilizes flexible regions on the periphery of the 50*S* subunit

(*A*) Central slice of local resolution maps of the unannealed, heated, and annealed 70*S* ribosomes. (*B–D*) Annealing stabilizes three typical flexible regions on the periphery of the 50*S* subunit. The positions of P1, P2, and P3 in 70*S* ribosomes are shown in Fig. 1*A*. Local resolution maps and histograms in the unannealed and annealed conditions are shown. Models were based on the annealed structures. Green and red arrows indicate the start and end, respectively, of selected strands.

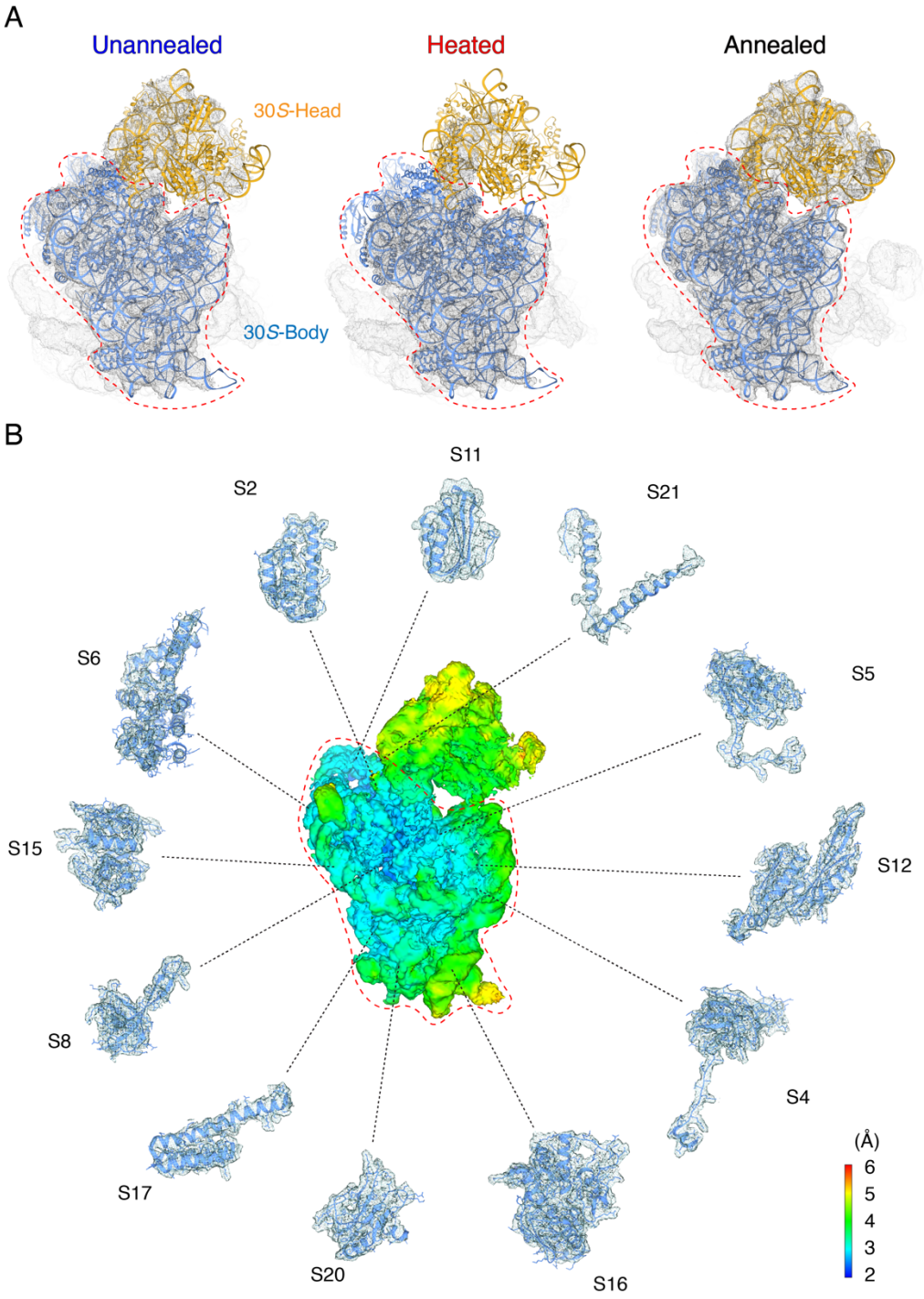

Figure S9. Modeling of 30S subunits from the unannealed, heated, and annealed ribosomes

(*A*) Docking of the atomic model of the 30*S* subunit into the unannealed, heated, and annealed ribosomes. The body domains of the 30*S* subunit were marked for high docking accuracy in all ribosomes. (*B*) Expanded view of peripheral proteins fitting into the body domain of the annealed 30*S* subunit.

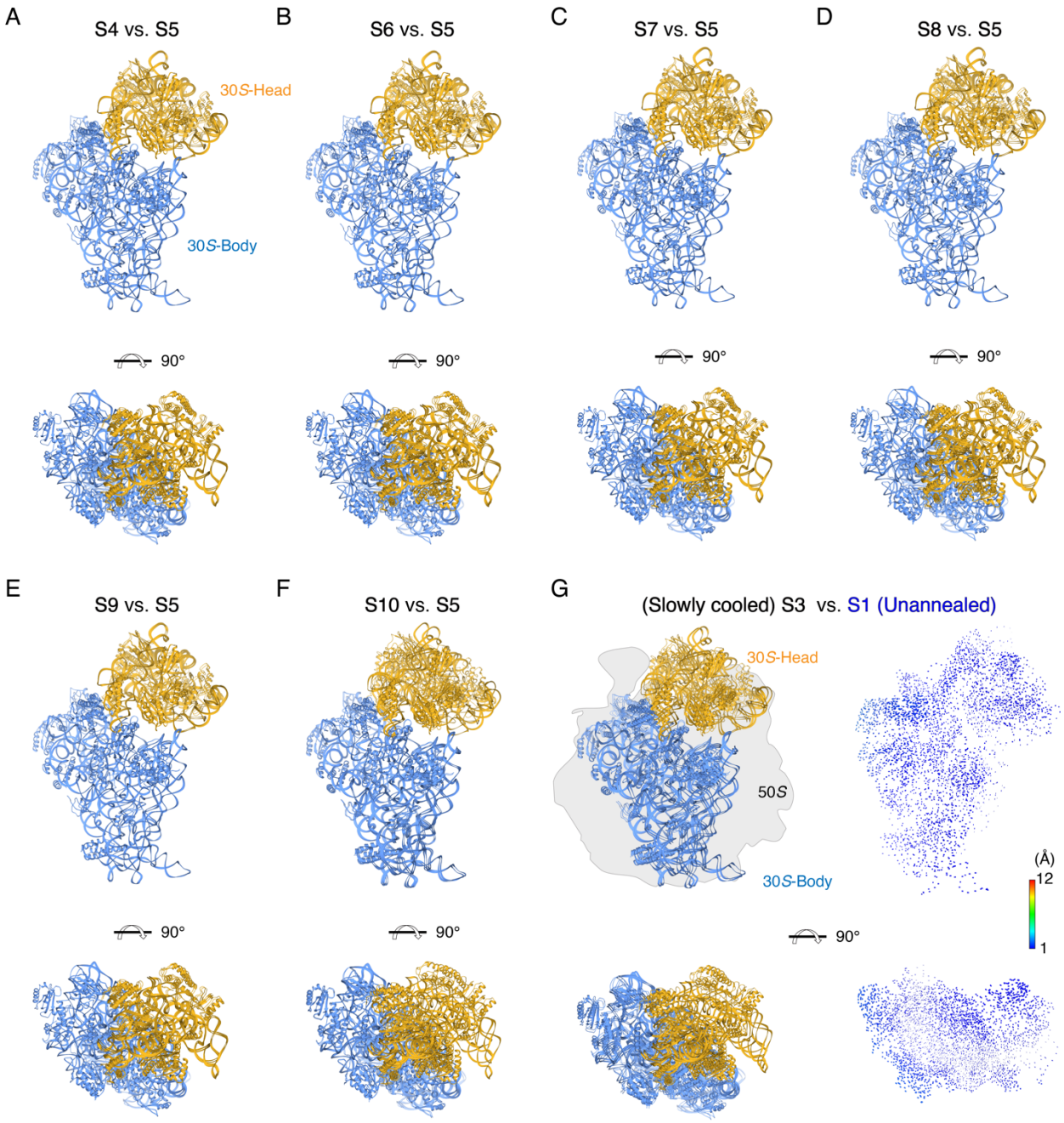

Figure S10. Rotational comparison of 30*S* subunits under various annealing conditions

(*A*–*F*) 50*S* subunits under various annealing conditions were aligned as the reference, and atomic models for the 30*S* subunits are shown. S1, S3, and S4–S10 correspond to annealing conditions as listed in Fig. 2*B*. (*G*) Rotational comparison of 30*S* subunits between slowly cooled and unannealed ribosomes. Left: Atomic models for the 30*S* subunits. Right: Difference vectors between phosphorous and Cα atoms in the 30*S* subunits.

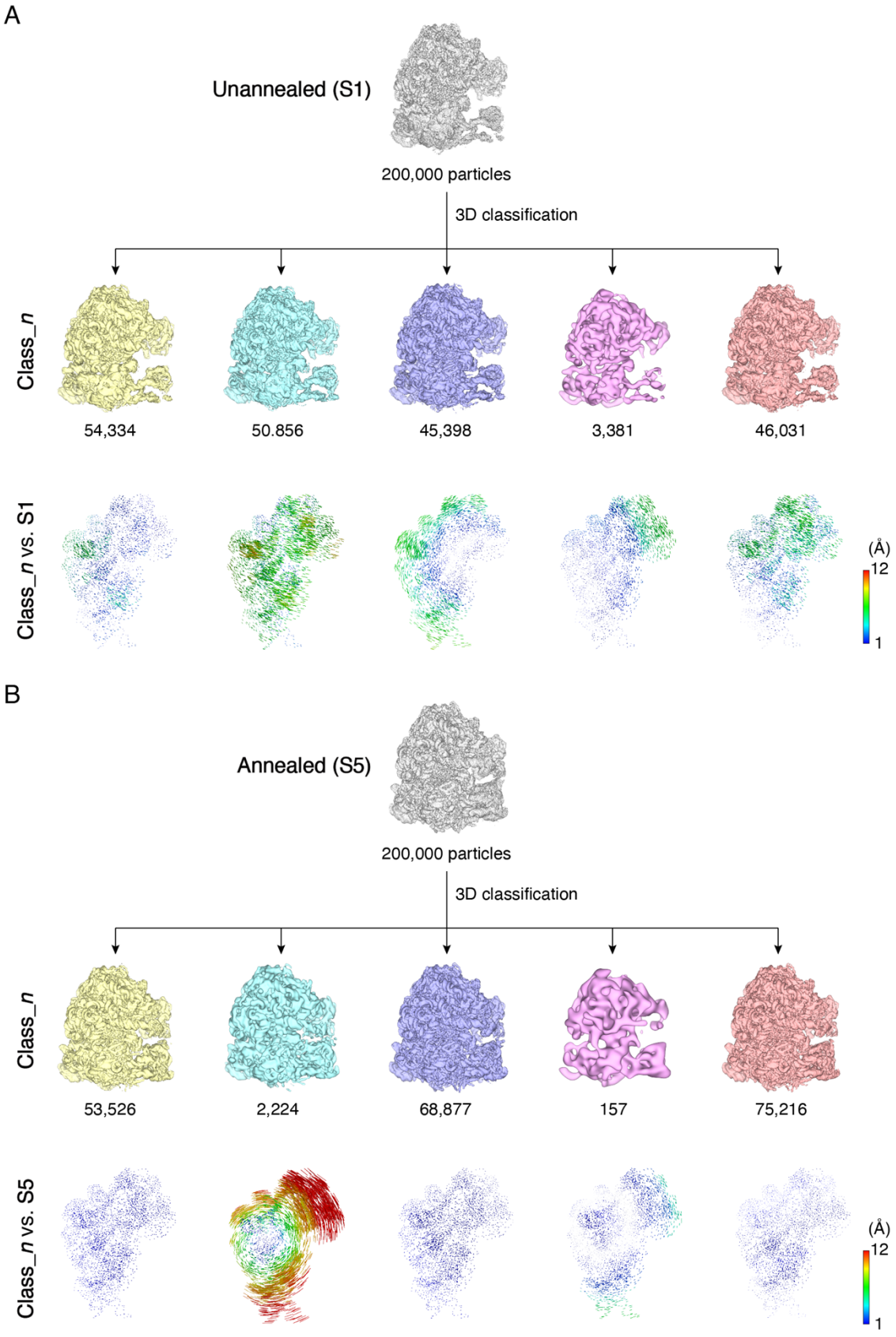
A
Unannealed (S1)
200,000 particles
3D classification
Class_n
54,334
50.856
45,398
3,381
46,031
Class_n vs. S1
(Å)
12
1
B
Annealed (S5)
200,000 particles
3D classification
Class_n
53,526
2,224
68,877
157
75,216
Class_n vs. S5
(Å)
12
1

Figure S11. Rotational comparison of 30*S* subunits between 70*S* ribosomes and their classified structures

(*A*) 3D classification of the unannealed 70*S* ribosome (S1) and the rotational comparison of 30*S* subunits between the annealed ribosomes and their classified structures. 50*S* subunits were aligned as the reference, and difference vectors between phosphorous and Cα atoms in the 30*S* subunits are shown. (*B*) 3D classification of the annealed 70*S* ribosome (S5) and the rotational comparison of 30*S* subunits between the annealed ribosomes and their classified structures. 50*S* subunits were aligned as the reference, and difference vectors between phosphorous and Cα atoms in the 30*S* subunits are shown.

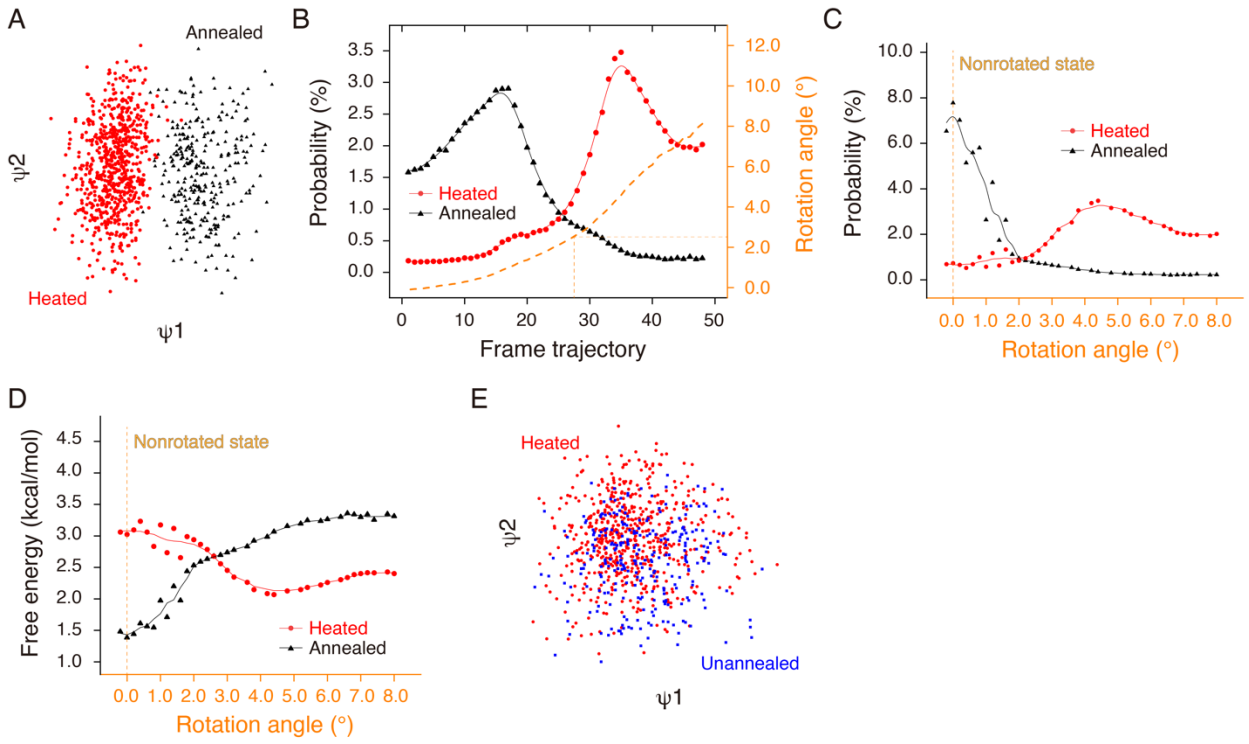

Figure S12. Free-energy minimization occurs during cooling from the heated ribosome to the annealed ribosome

(*A*) Initial manifold snapshots of the 70*S* ribosome in one projection direction. The points are colored in accordance with the heated and annealed subsets. The projection direction is approximately orthogonal to the interface between the 50*S* and 30*S* subunits. (*B*) Particle distribution of the heated and annealed ribosomes along the frame trajectory. The 3D structure at each frame was reconstructed, and the rotation angle of 30*S* subunit with respect to the nonrotated state was calculated. (*C*) Particle distribution of the heated and annealed ribosomes along the rotation angle. Particle distribution was recalculated with the rotation angle at an interval of 0.2°, and a moving average was used to smooth the data variation. (*D*) Free-energy distribution of the heated and annealed ribosomes along the rotation angle. The free energy was calculated from the fitted curve in (*C*). The free energy for heated and annealed ribosomes was calculated via the Boltzmann formula with the respective temperature at 310 K and 273 K. (*E*) Initial manifold snapshots of the 70*S* ribosome in one projection direction. The points are colored in accordance with the unannealed and heated subsets. It is challenging to efficiently separate two states.

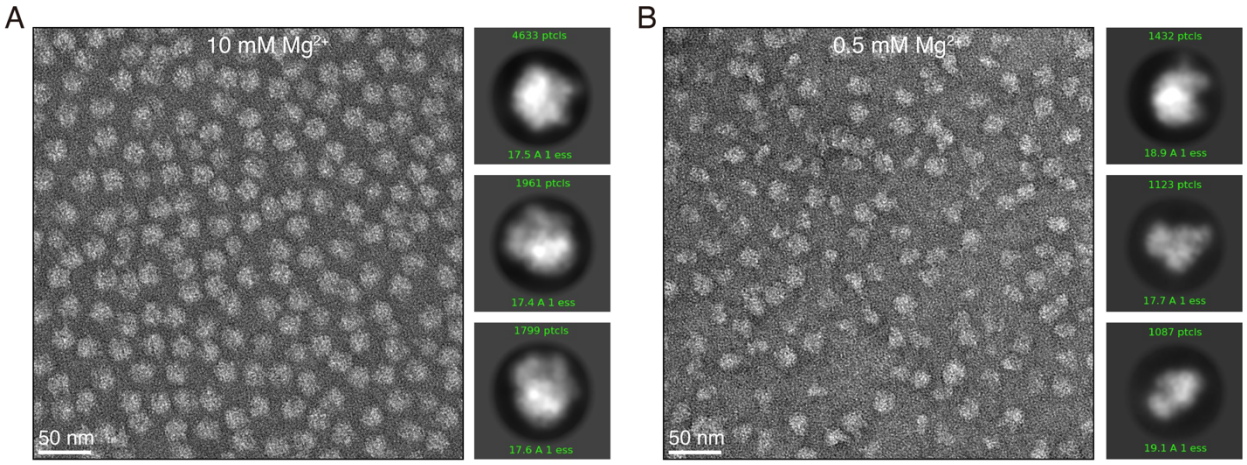

Figure S13. 70*S* ribosome dissociates at 0.5 mM Mg^{2+} concentration

(*A*) Typical negative-stain image and the 2D class average of the 70*S* ribosome at 10 mM Mg^{2+} concentration. (*B*) Typical negative-stain image and the 2D class average of the 70*S* ribosome at 0.5 mM Mg^{2+} concentration.

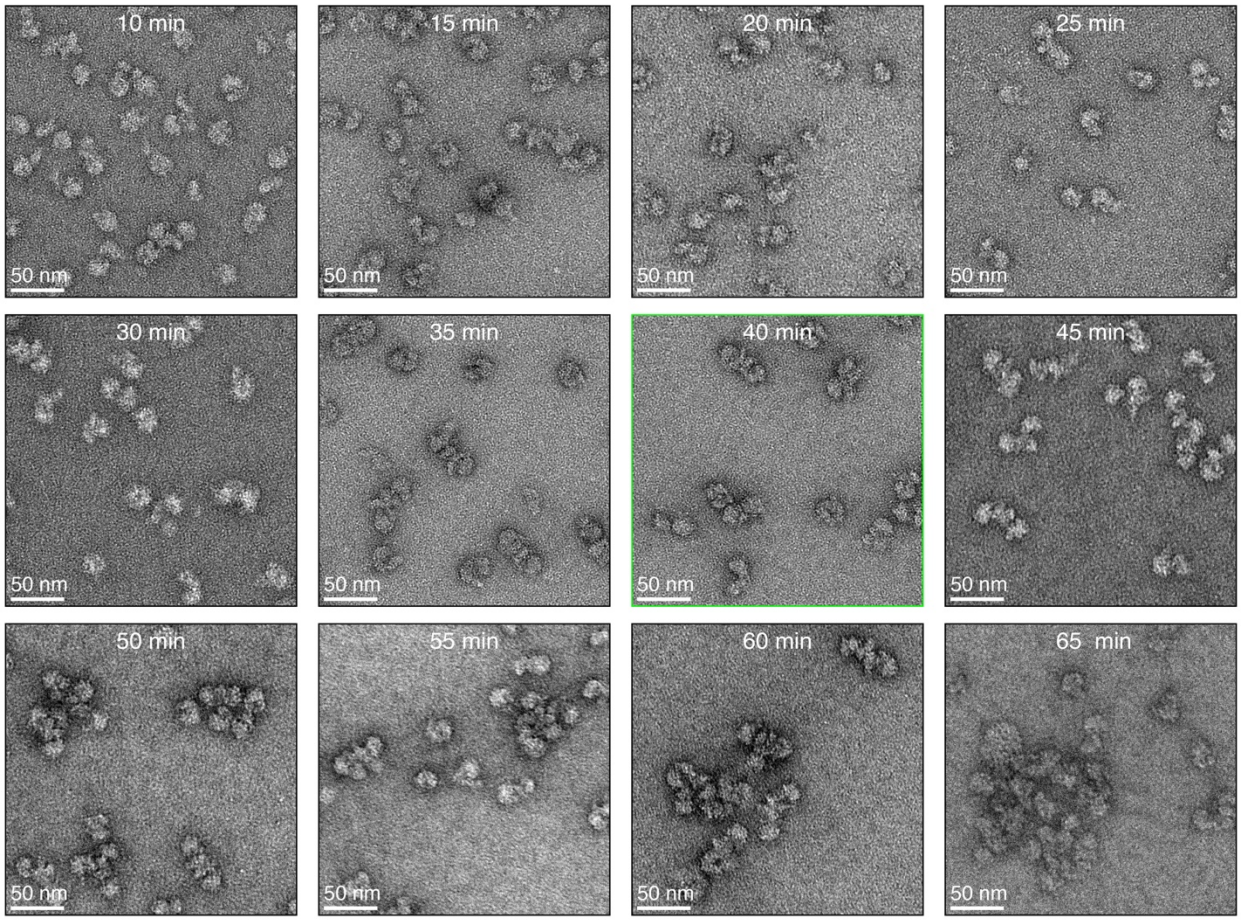

Figure S14. Glutaraldehyde cross-links 70*S* ribosome from dissociation at 0.5 mM Mg^{2+} concentration

A series of negative-stain images at various GA cross-linking times. After 40 min of cross-linking, the 70*S* ribosome will not dissociate at 0.5 mM Mg^{2+} concentration. An even longer cross-linking time will incur the 70*S* ribosome into clusters or aggregates.

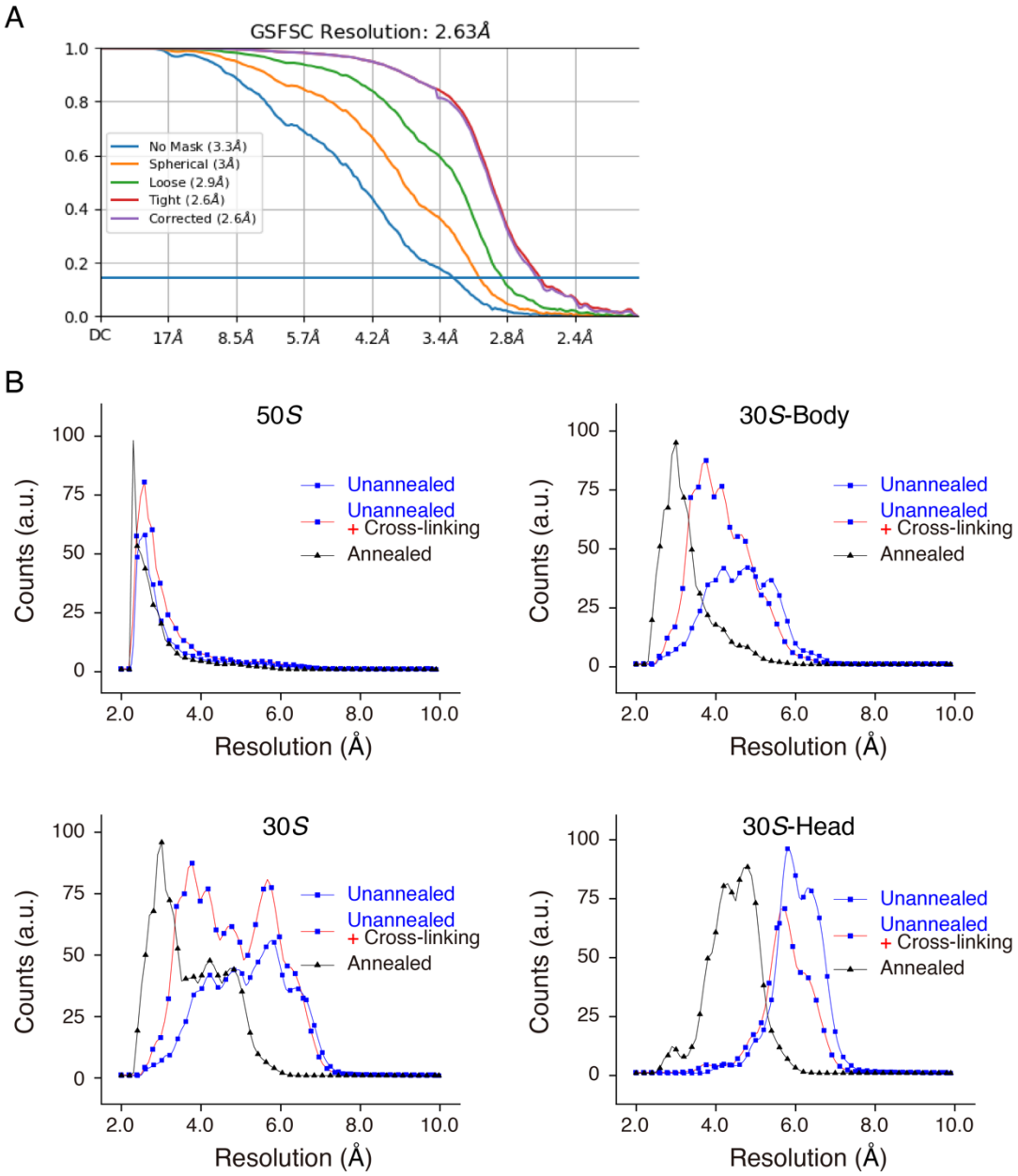

Figure S15. FSC curve and local resolution histograms of the unannealed ribosome after GA cross-linking

(*A*) FSC curve for the GA cross-linked ribosome. (*B*) Local resolution histograms of the GA cross-linked ribosome. The mean and standard deviation from these histograms were calculated (*SI Appendix*, Fig. S16*B*).

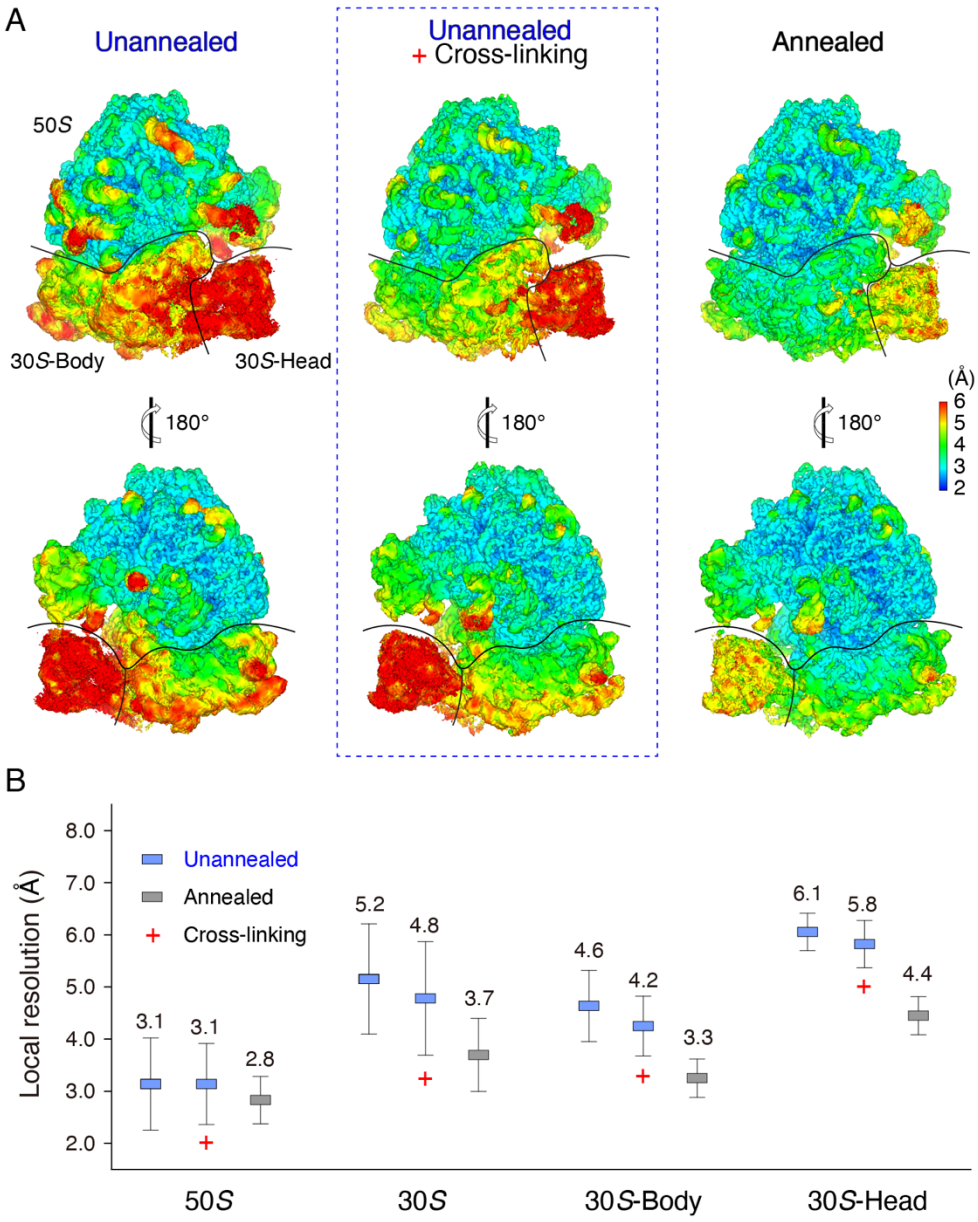

Figure S16. The effect of GA cross-linking on the unannealed ribosome

(*A*) Structural comparison between the GA cross-linked ribosome and the unannealed/annealed ribosomes. For direct comparison, local resolution maps of unannealed and annealed 70*S* ribosomes are re-used from Fig. 1. The GA cross-linked ribosome is marked in the dashed rectangle. (*B*) Local resolution comparison of the GA cross-linked ribosome with the unannealed/annealed ribosomes. The respective means and standard deviations were calculated from *SI Appendix*, Fig. S15*B*.

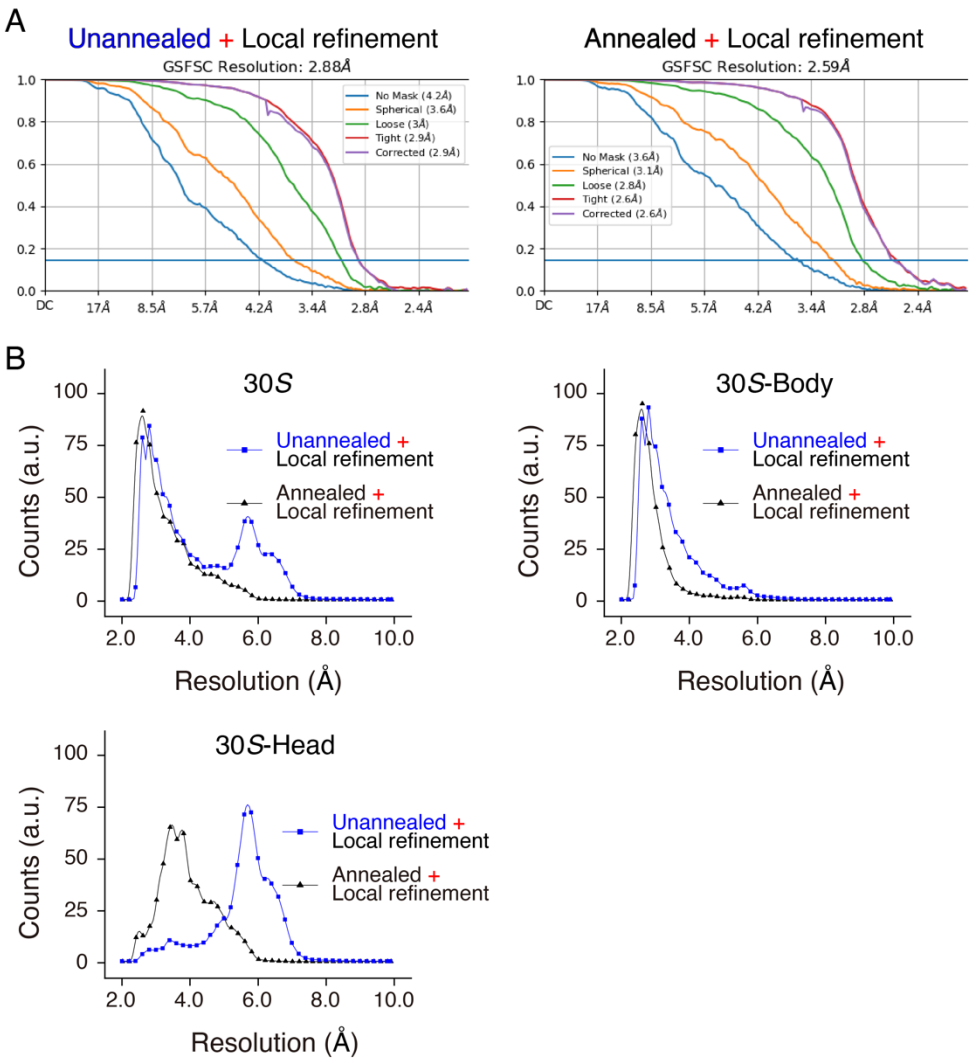

Figure S17. Resolution estimation of 30S subunits after local refinements

(*A*) FSC curves for 30*S* subunits after local refinements on unannealed and annealed ribosomes. (*B*) Local resolution histograms of the 30*S* subunit and subdomains after local refinements on unannealed and annealed ribosomes. The mean and standard deviation from these histograms were calculated (*SI Appendix*, Fig. S18*B*)

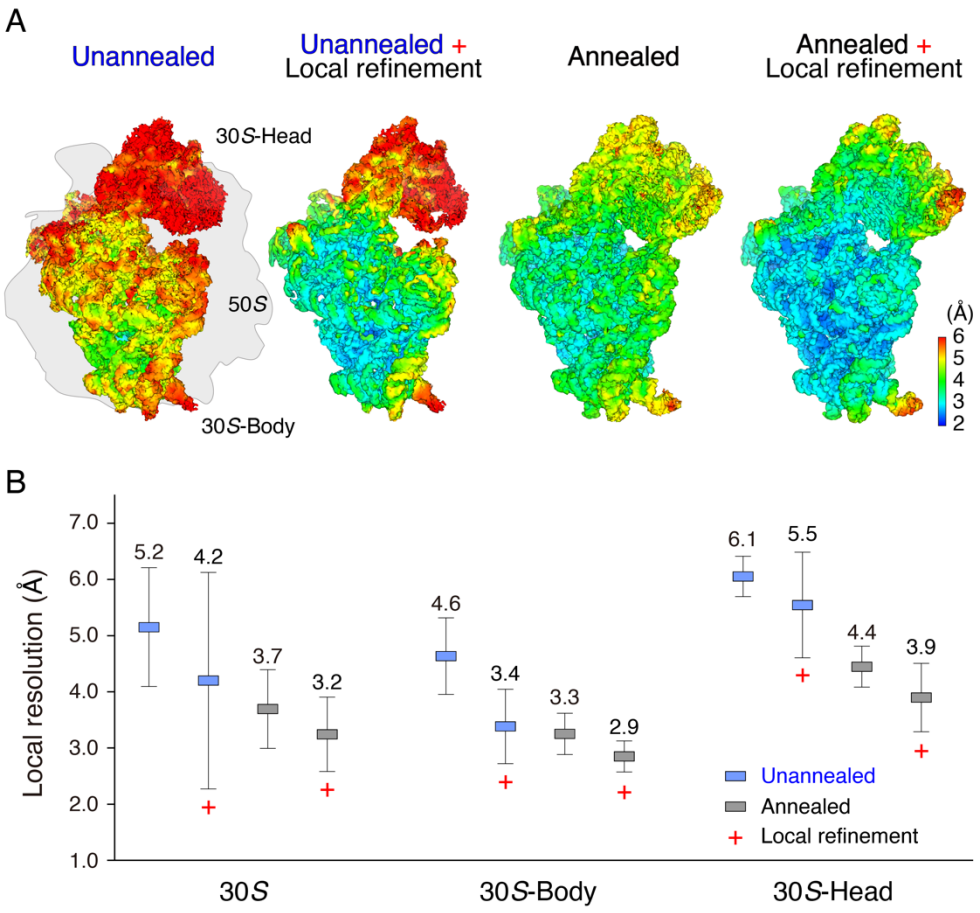

Figure S18. Structural comparison of 30*S* subunits before/after local refinements

(*A*) Local resolution maps of 30*S* subunits under various conditions. (*B*) Local resolution comparison of unannealed and annealed 30*S* subunits before/after local refinements. The respective means and standard deviations were calculated from *SI Appendix*, Fig. S17*B*.

Table S1. Cryo-EM data collection and data processing statistics

	Heated ribosome (S2)	Unannealed (S1) and annealed (S3–S10) ribosomes
Sample preparation		
Concentration (nM)	700	700
Loading volume (μL)	4.5	4
Chamber temperature (°C)	37	4
Chamber humidity (%)	100	100
Blot time (s)	0.5	0.5
Blot force	−5	−2
Data collection and processing		
Microscope	Titan Krios G^{3i}	
Voltage (kV)	300	
Camera	Gatan K3 BioQuantum	
Magnification	81,000	
Electron exposure (e^{-}/Å^2)	60	
Defocus range (μm)	1.0–1.5	
Pixel size (Å)	0.53	
Symmetry imposed	C1	
Initial particle images (no.)	*SI Appendix*, Fig. S2*B*	
Final particle images (no.)	*SI Appendix*, Fig. S2*B*	
Map resolution (Å)	*SI Appendix*, Fig. S3	
FSC threshold	0.143	
Map resolution range (Å)	*SI Appendix*, Fig. S6	

Movie S1. Cartoon that illustrates how to use the mist umbrella

Movie S2. Typical movies for structural variation of the unannealed, heated, and annealed ribosomes